Journal of *Marine Science and Engineering*

MDPI

Article

Experimental Validation of a Fast-Tracking FOCV-MPPT Circuit for a Wave Energy Converter Embedded into an Oceanic Drifter

Matias Carandell [1,*], Daniel Mihai Toma [1], Andrew S. Holmes [2], Joaquín del Río [1] and Manel Gasulla [1]

[1] Electronic Engineering Department, Universitat Politècnica de Catalunya, 08800 Vilanova i la Geltrú, Spain; daniel.mihai.toma@upc.edu (D.M.T.); joaquin.del.rio@upc.edu (J.d.R.); manel.gasulla@upc.edu (M.G.)
[2] Department of Electrical and Electronic Engineering, Imperial College London, London SW7 2AZ, UK; a.holmes@imperial.ac.uk
* Correspondence: matias.carandell@upc.edu; Tel.: +34-938967208

Abstract: Wave Energy Converters (WECs) are an ideal solution for expanding the autonomy of surface sensor platforms such as oceanic drifters. To extract the maximum amount of energy from these fast-varying sources, a fast maximum power point tracking (MPPT) technique is required. Previous studies have examined power management units (PMU) with fast MPPT circuits, but none of them have demonstrated their feasibility in a real-world scenario. In this study, the performance of a fast-tracking fractional open circuit voltage (FOCV)-MPPT circuit (sampling period T_{MPPT} of 48 ms) is compared with a commercial slow-tracking PMU (T_{MPPT} of 16 s) in a monitored sea area while using a small-scale, pendulum-type WEC. A specific low-power relaxation oscillator circuit is designed to control the fast MPPT circuit. The results demonstrate that by speeding up the sampling frequency of the MPPT circuit, the harvested energy can be increased by a factor of three.

Keywords: energy harvesting; fractional open circuit voltage; maximum power point tracking; oceanic drifter; power management unit; wave energy converter

Citation: Carandell, M.; Toma, D.M.; Holmes, A.S.; del Río, J.; Gasulla, M. Experimental Validation of a Fast-Tracking FOCV-MPPT Circuit for a Wave Energy Converter Embedded into an Oceanic Drifter. *J. Mar. Sci. Eng.* **2023**, *11*, 816. https://doi.org/10.3390/jmse11040816

Academic Editors: Hao Wang, Minyi Xu and Xinxiang Pan

Received: 7 March 2023
Revised: 6 April 2023
Accepted: 8 April 2023
Published: 11 April 2023

1. Introduction

Global awareness has forced policy-makers to address the protection of marine areas in order to mitigate the effects of human activities, such as abusive fishing, excessive industrial production and poorly-optimized global transportation. In order to quantify the effectiveness of these policies, there is an urgent need to improve our understanding of marine ecosystems. Technology, and, more specifically, sensor platforms, must play a central role in developing monitoring systems to better understand and predict ocean changes.

Oceanic drifters are autonomous, floating sensor platforms, used in marine climate research to monitor surface ocean currents, as well as other sea-surface parameters such as temperature and salinity. They are low-cost, versatile and easy-to-deploy instruments, so many of them can be deployed to cover large oceanic regions. Energy autonomy is a challenging factor in the design of drifters. The ability to operate autonomously over extended periods of time is crucial in order to reduce the costs associated with exchanging batteries in the middle of the ocean. For this reason, some manufacturers include photovoltaic (PV) panels around the drifter's shell, achieving unlimited autonomy; however, this is not an ideal solution. Drifters strictly dedicated to monitoring superficial ocean currents should not be exposed to wind because it may compromise current tracking [1]. Consequently, they must be mostly submerged, which interferes with the availability of solar energy. For this reason, other energy sources are being explored, such as harvesting the kinetic energy of the ocean surface with energy harvesting (EH) transducers, specifically by using mechanical-to-electrical devices such as wave energy converters (WECs).

Pendulum-type WECs have proven to be a suitable solution to harvest energy from the ocean surface [2]. The design of such systems for drifters is challenging because the

articulated moving mass could affect the motion of the drifter itself, and thus interfere with its data collection. However, as noted in [3], as long as the articulated mass does not exceed a certain percentage of the total weight, the mechanical-to-electrical conversion of the drifter's energy can be satisfactorily achieved. Several studies on pendulum-type WECs harvesting energy from small-size free-floating buoys (e.g., drifters) with both electromagnetic and piezoelectric devices have been published since 2019. An electromagnetic converter was reported in [4] which captured the energy from the relative motion of a drogue (50 cm diameter) and the drifter, generating tens of milliwatts of average power. The results were based on simulations of random waves, with a peak frequency of 1 rad/s and a significant height of 2 m. An electromagnetic-based swing body ($10 \times 10 \times 6.3$ cm^3) was presented in [5] with experimental results reporting peaks of 0.13 W in the ocean under wave heights which peaked at 0.8 m. Feng et. al. presented in [6], a hybrid nanogenerator integrating triboelectric, piezoelectric, electromagnetic, photovoltaic and thermotropic units to harvest ocean ambient energy and feed a 14 cm diameter buoy. A peak power of 13.8 mW was achieved with the electromagnetic unit using a linear motor excited at 2.4 Hz. Back in 2021, we reported in [7] an electromagnetic, small-size, pendulum-type WEC that harvested energy from a drifter and achieved approximately 0.2 mW of average useful power. Finally, a chaotic pendulum with a hybrid system, including a triboelectric and an electromagnetic module, was presented in [8], that extracted the kinetic energy of a small-size moored buoy, reaching an average output power of 15 μW and 1.23 mW, respectively, for each technology. A linear motor with an excitation frequency of 2.5 Hz was used. Although all the average harvested power levels were low (<100 mW), they may be enough to feed low-power instrumentation that spends most of its life sleeping but powers up several times per day to acquire and transmit the desired ocean parameters. A common characteristic in [4–8] is that the WEC device's output oscillates not at the wave frequency, but at the motion frequency of the drifter (f_{EH}). According to [9], for a small-size drifter (20 cm diameter and 3.6 kg), f_{EH} is around 1.6 Hz and 1 Hz in the horizontal and vertical axes, respectively, under the influence of waves, with an average frequency of 0.37 Hz (both values can be obtained with Equations (7) and (8) from [10]). A power management unit (PMU) is then required at the WEC's output to convert its variable signal into a constant and clean supply to feed the drifter's electronics (load). PMUs must also manage any power mismatch between the WEC and the load by including an energy storage element (ESE) where energy can be stored or dispatched as required. Finally, PMUs usually include a maximum power point tracker (MPPT) to continuously ensure the maximum available energy is harvested from the WEC.

One simple MPPT technique, widely used for low-power EH transducers, is the fractional open circuit voltage (FOCV) method [11]. This method exploits the linear relationship between the maximum power point (MPP) voltage (V_{MPP}) and the open circuit voltage (V_{OC}) of the EH transducer. MPP is achieved by fixing the output voltage of the EH transducer to the V_{MPP}, which is a percentage of its V_{OC} (50% for electromagnetic or piezoelectric harvesters). Typically, V_{OC} is sampled (at a sampling period T_{MPPT}) by momentarily disconnecting the EH transducer from the PMU during a sampling time (t_{SAMP}). The sampling period should be significantly shorter than the motion period T_{EH} (=$1/f_{EH}$), i.e., $T_{MPPT} << T_{EH}$ or $f_{MPPT} >> f_{EH}$, while at the same time being much longer than the sampling period, i.e., $t_{SAMP} << T_{MPPT}$.

Popular commercial PMU ICs, such as the BQ25504/5 (Texas Instruments, Dallas, TX, USA) or the ADP5091/2 (Analog Devices, Willmington, NC, USA), use the MPPT-FOCV technique but fail to provide sufficiently high sampling rates for WECs. Some academic works have achieved fast sampling rates and low sampling times: t_{SAMP} = 5 ms/T_{MPPT} = 100 ms [12], 33 μs/3.33 ms [13], 15 ms/1 s [14] and 10 ms/150 ms [15]. However, none of them theoretically analyzes the effect of the sampling parameters (T_{MPPT}, t_{SAMP}) on the harvested power. Refs. [16,17] address this issue for FOCV-MPPT techniques. In contrast, in [16], Balato et al. optimized the parameters of the FOCV method to maximize the power extracted from resonant piezoelectric vibration harvesters after an AC/DC bridge rectification step.

However, the parameter t_{SAMP} was kept constant to 0.3 s in the analysis and only variations in T_{MPPT} were considered. Furthermore, in [17] we reported that when $f_{EH} = 15 \cdot f_{MPPT}$, 99% of the maximum energy is harvested. Theoretical predictions were confirmed using a self-designed FOCV-MPPT circuit and a WEC excited in a linear shaker.

In this paper, the performance of the fast-sampling FOCV-MPPT circuit (specifically config. C presented in [17]) is validated for real-world application by experimental testing in the sea. This is something that, to the best of our knowledge, has not been assessed before. The small-size drifter with a whole power measurement system and the small-size, double-pendulum WEC previously presented in [7] are used for this purpose. Furthermore, a low-power control circuit was designed, simulated and tested to implement the sampling signal of the MPPT technique. This paper is organized as follows: Section 2 presents the whole EH system including the WEC device, the PMU with the FOVC-MPPT circuit and the ESE. Section 3 describes the experimental testing methodology and Section 4 presents the results. Section 5 concludes the work.

2. Description of the EH System

Figure 1 shows a block diagram of an autonomous sensor platform that uses an EH system to feed its load. For a drifter, the load mainly includes sensors and their electronic interfaces, a microcontroller, and wireless modules for GPS and satellite data transfer. The EH system consists of an EH transducer (WEC), a PMU and an ESE (a rechargeable battery in Figure 1). The PMU provides a regulated voltage output to the load, performs the MPPT and interacts with the ESE. In this section, the EH system components used are described.

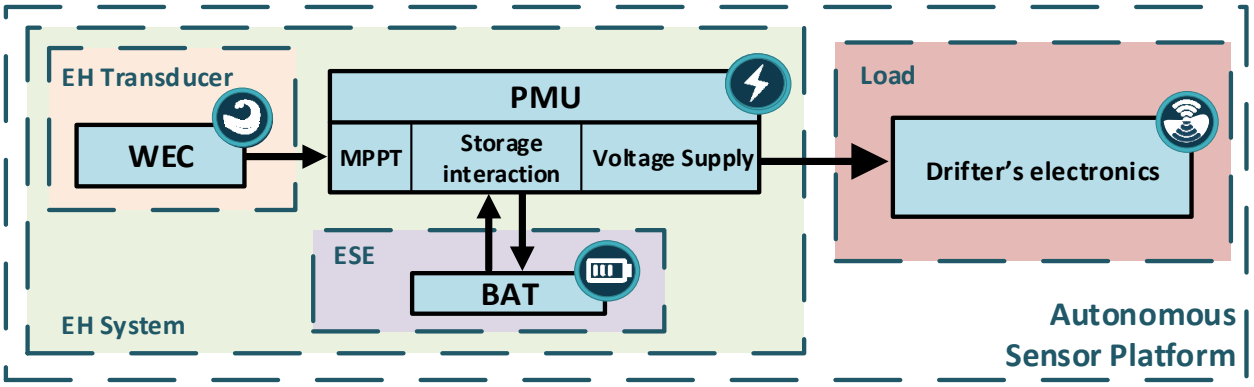

Figure 1. Autonomous Sensor Platform configuration; the load represents the drifter's electronics, while the EH system includes the EH transducer (WEC), the PMU and the ESE.

2.1. Wave Energy Converter (WEC)

2.1.1. Mechanical Device

The WEC is shown in Figure 2 (left). It consists of a double pendulum containing an arm with a proof mass guaranteeing the alignment of the main body with the wave's direction. The arm is articulated to a ring (main body) which, in turn, is articulated to the drifter, so its participation is relative to the ring's oscillation. A gear train is coupled to the ring. Through that train, energy is accumulated in a flywheel that drives a DC electrical generator. The gear system amplifies the angular velocity with a positive ratio of 35 and, thanks to a one-way bearing, the unidirectional rotation of the electrical generator is ensured. The WEC's total mass and diameter are 0.12 kg and 12 cm, respectively; the rest of constructive parameters are fully described in [7].

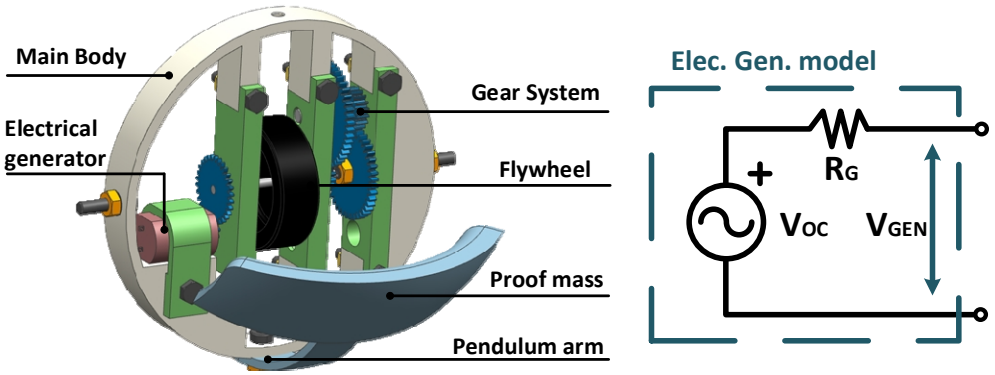

Figure 2. WEC transducer with the description of its main components (**left**, [7]) and its electrical model (**right**).

2.1.2. Electrical Generator and Model

The WEC's electrical generator is a brushless DC motor, which can be modelled as a Thévenin equivalent circuit, as presented in Figure 2 (right). V_{GEN} is the generator's output voltage, R_G is the internal equivalent resistance and V_{OC} is the generated electromotive force given by

$$V_{OC} = K_G \varphi \omega, \quad (1)$$

where K_G is the motor constructive constant, φ is the magnet field generated by the permanent magnet, and ω is the generator rotor speed. Maximum power at the output is achieved when $V_{GEN} = 0.5V_{OC}$ ($= V_{MPP}$), as stated by the maximum power transfer theorem [18]. Since K_G and φ are constants, V_{OC} is proportional to ω. Within one single pendulum cycle, when the pendulum applies torque through the one-way gear, the flywheel accelerates, increasing ω, and thus V_{OC}, whereas when the pendulum moves in the other direction, the one-way gear rotates freely, so that the flywheel slows down, thus reducing ω and V_{OC}. Therefore, V_{OC} will have both DC and AC components, even for a constant excitation source. The AC component will be periodic, with the same frequency as the mechanical movement of the pendulum, and thus of the drifter. According to the WEC's characterizations made in [7], the internal series resistor R_G is 127 Ω.

2.2. Power Management Unit

2.2.1. MPPT-FOCV Circuit

The FOCV is an MPPT method widely used in low-power EH transducers and implemented in several commercial PMU Ics. This method exploits the linear relationship between V_{MPP} and V_{OC} of the EH transducer. For the WEC, $V_{MPP} = 0.5V_{OC}$, as shown in Section 2.1.2. Typically, V_{OC} is periodically measured with a sample and hold (S&H) circuit by momentarily disconnecting the EH transducer from the PMU. Figure 3 shows the principle of operation of a FOCV circuit tracking the MPP of a sinusoidal V_{OC} (black line) with a period of T_{EH}. V_{MPP} is shown in gray. Every sampling period (T_{MPPT}), the sampling circuit opens the EH transducer's output during t_{SAMP} so that V_{GEN} (blue dashed line) raises to V_{OC}. At the end of t_{SAMP}, V_{GEN} is fixed to the new MPP value (e.g., V_{MPP1}) derived from the last captured value of V_{OC} (e.g., V_{OC1}) during t_{HARV}, which is the harvesting time and corresponds to the rest of the sampling period.

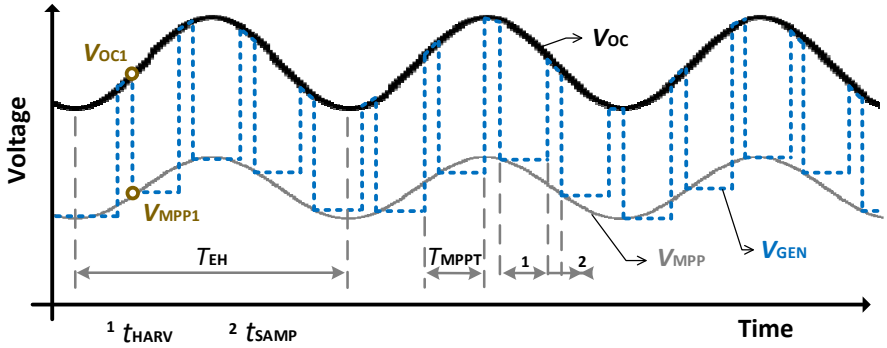

Figure 3. Sinusoidal V_{OC} waveform with positive offset for a harvester (black line), the corresponding ideal V_{MPP} ($\frac{1}{2}V_{OC}$: gray line) and the EH output (V_{GEN}: blue line) for a T_{MPPT} sampling period using the FOCV-MPPT method.

The FOCV-MPPT method is commonly implemented with a resistor-based S&H circuit, where a resistor divider is used to generate the desired fraction of V_{OC} and then store it in a sampling capacitor C_{SAMP} [12]. In this study, this configuration is implemented with the ADP5092 PMU IC (config. R), which presents a low sampling rate, and is compared with a novel configuration with a high sampling rate, presented in [17] as config. C (Figure 4). Config. C also uses the ADP5092 IC in order to take advantage of its robustness and power efficiency, but adds low-power sampling circuitry to drastically increase the sampling rate to implement a slight variation over the classical FOCV method. The WEC (orange box) is represented with the Thévenin model of Figure 2 (right). The working principle is that during t_{SAMP}, S_{12} connects V_{GEN} to an impedance reference R_Z (=R_G = 127 Ω), so that V_{DIV} (junction of R_Z with the WEC) samples V_{MPP} in C_{SAMP}, which is $V_{OC}/2$. Thus, the WEC must have already been configured to know R_G, and this value should not change significantly over time. During t_{HARV}, S_{12} connects V_{GEN} to V_{IN}, disconnecting R_Z, and fixes it to the new V_{MPP}. Given R_Z is much smaller than the common resistor divider values used in FOCV circuits (normally tens of MΩ), t_{SAMP}, and thus T_{MPPT} can be drastically reduced, allowing for a fast-sampling rate. The physical limitations of these parameters are fully described in [17], as are the values of the different circuit components for both config. R and config. C. Eight test points are used for the analysis of the PMU performance. V_{GEN}, V_{BAT}, I_{IN} (input current), I_{OUT} (output current), V_{DIV}, V_{MPP}, V_{IN} and V_{PULSE} (sampling control signal for the switches).

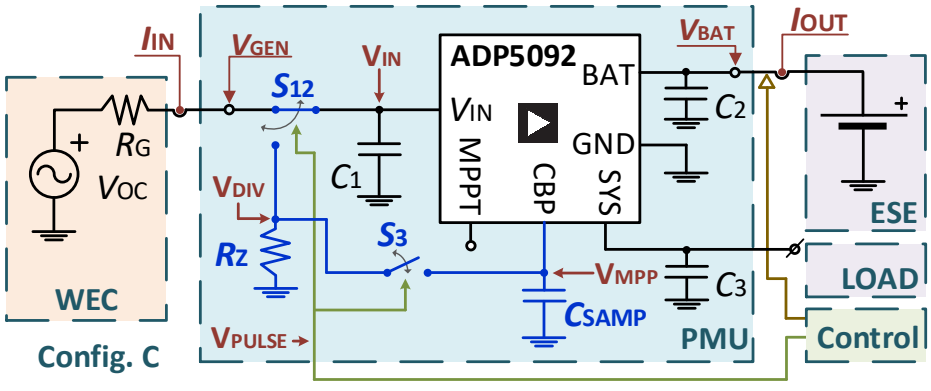

Figure 4. FOCV-MPPT config. C circuit presented in [17], together with the WEC's electrical model as the input source and an ESE as the sole output load.

Config. C performance relies on the previous knowledge of the WEC R_G, which then fixes R_Z. R_G and R_Z (=R_G) set the resistor divider used to sample $V_{OC}/2$. A relative change α (<<1) in either R_G (e.g., by time drift or inaccurate characterization) or R_Z (e.g., by the tolerance or temperature drifts) leads to a relative error of $\alpha/2$ in the correct determination

of V_{MPP}. As simple calculations show, this results in a relative change of $\alpha^2/4$ on the power provided by the WEC. For example, when $\alpha = 0.01$ (1%), the power imperceptibly decreases by 0.0025%. A relatively larger α of 0.1 (10 %) results in a power decrease of just 0.25%. Thus, the circuit is very tolerant to changes in R_G and R_Z.

2.2.2. Sampling Control Circuit and Timings

The results reported in [17] were obtained in the laboratory, either by emulating the WEC signal with a function generator or by exciting the WEC with a linear shaker. The control signal V_{PULSE} was provided by a commercial DAQ. In this study, where the tests were performed in the sea, the design of a low-power circuit to generate V_{PULSE} was required.

Figure 5 shows the implemented circuit based on a relaxation oscillator (RO) using two comparators and with the appropriate resistive and capacitive components (R_{21}, R_{22}, R_{23}, C_{21} and C_{22}). The first stage generates a squared wave (V_A) whereas the second stage generates a pulse train, V_{PULSE}, where

$$T_{MPPT} = 2R_{21}C_{21}\ln\left(\frac{m+1}{m}\right) \quad (2)$$

$$t_{SAMP} = \frac{mR_{22}C_{22}}{m+1}\ln\left(\frac{2m}{m+1}\right) \quad (3)$$

and

$$m = \frac{R_{23}}{R_{22}} \quad (4)$$

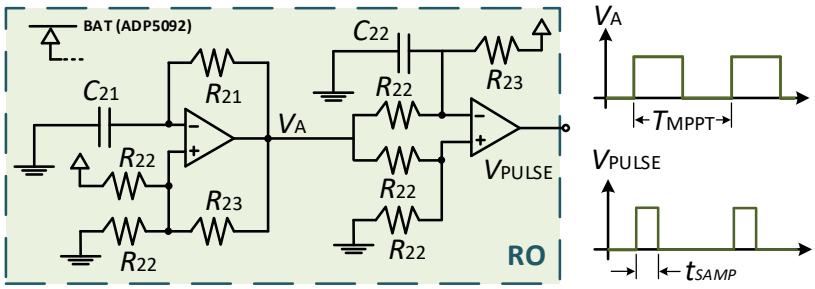

Figure 5. Relaxation oscillator (RO) for the generation of V_{PULSE}.

The circuit is powered from the ESE in such a way that the derived current is subtracted from I_{OUT}, and so the related losses are accounted for in the PMU power efficiency. Using the MCP6542 IC for both comparators, the consumption of this circuit could be kept to below tens of microwatts. The components and values used for the RO circuit are detailed in Table 1.

Table 1. Component list for the relaxation oscillator.

CMP	R_{21}	R_{22}	R_{23}	C_{21}	C_{22}
MCP6543 [1]	1.2 MΩ	1 MΩ	1.2 MΩ	33 nF	1.2 nF

[1] This IC includes both CMP.

Table 2 reports the sampling parameters (t_{SAMP} and T_{MPPT}) for both configurations used in the test. The parameters of config. R are fixed by the PMU IC and provide a slow sampling rate. The parameters of config. C result from (2) to (4), using the values of Table 1. The justification for this selection is found in Section 4. Table 2 also includes the sample ratio defined in [17], $r_S = \frac{t_{SAMP}}{T_{MPPT}}$, to describe the percentage of time the PMU is sampling over the total time. Notice a lower value of r_S has been used in config. C than in config. R, further increasing the harvesting time, and thus the harvested power.

Table 2. Sampling parameters for each configuration.

Config	t_{SAMP}	T_{MPPT}	r_S
C	57 µs	48 ms	0.12%
R	256 ms	16 s	1.6%

The RO circuit with the components reported in Table 1 was simulated in Multisim (National Instruments). The results (Figure 6) confirm the parameters obtained in Table 2.

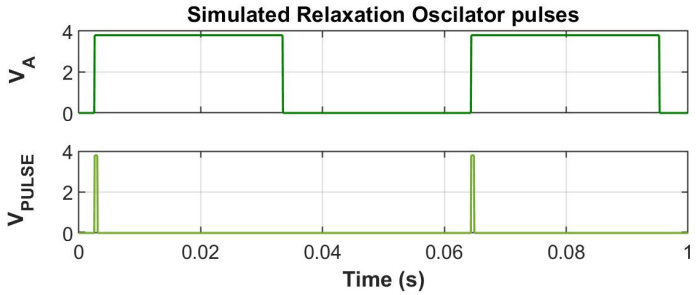

Figure 6. Simulated RO pulses with Multisim.

2.3. Energy Storage Element and Load

For the ESE, a 165 mAh—3.7 V Li-Ion polymer battery charged at 3.8 V was selected. No load is connected to the SYS pin, so that the output power is only delivered to the ESE, and thus the estimation of the PMU efficiency is simpler.

3. Experimental Setup

A 20 cm spherical drifter with no outer ring (WAVY Ocean from MELOA consortium [19], shown in Figure 7) was used to embed the whole or part of the EH systems described in Section 2 (WEC, PMU and ESE), jointly with a measurement system. The drifter was properly weighted to 3.6 kg, with the appropriate ballast to minimize the exposure of the surface to the wind while maintaining its buoyancy. The mass center of the drifter was located in the lower hemisphere to ensure vertical alignment.

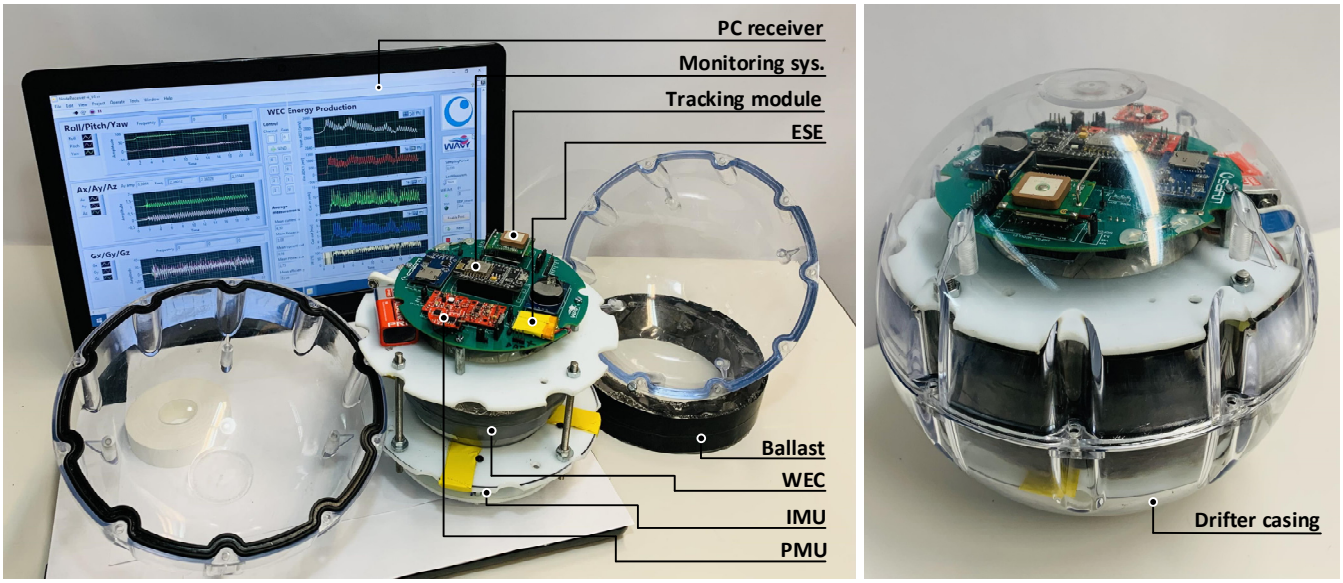

Figure 7. Experimental set-up for the tests. (**Left**) the EH and monitoring systems with the two semi-spheres of the drifter, the ballast and the PC receiver. (**Right**) spherical drifter casing with the EH and monitoring systems embedded.

The wireless measurement system, which was expressly developed for drifters in [7], allows real-time monitoring and includes an inertial measurement unit (IMU) placed at the drifter's mass center to estimate its linear accelerations (A_X, A_Y and A_Z), a four-channel analog-to-digital converter (ADC) to measure V_{GEN}, V_{BAT}, I_{IN} and I_{OUT} (Figure 4), and an ESP8266-based microcontroller to control the subsystems, and acquire and transmit the data. Input and output powers to the PMU can be estimated as $P_{IN} = V_{GEN} \cdot I_{IN}$ and $P_{OUT} = V_{BAT} \cdot I_{OUT}$, respectively. A SigFox-based GPS tracking module was also included to recover the unit in case of loss. The whole measurement system was powered by an external battery, avoiding any energy interference with the EH system.

Two tests were performed by deploying the drifter in the sea at a location 4 km offshore from Vilanova i la Geltrú harbour, Spain, near the underwater seafloor observatory OBSEA [20], which is a fishing-protected and monitored area (Figure 8). Measurements were performed every 20 ms and wirelessly transmitted to a laptop placed in a nearby boat that used in the test. In both tests, the WEC with the measurement system was embedded into the drifter. In the first test, the WEC's output was placed in open circuit, and V_{OC} and the system accelerations were measured. The objective of this test was to estimate f_{EH} from the movement of the drifter under the effect of ocean waves in order to choose an appropriate value of f_{MPPT} ($\geq 15 f_{EH}$, according to [17]). The second test also included the PMU and ESE in order to compare the performance of configs. R and C. Both MPPT configurations were tested consecutively in the same drifter. For this test, the input and output voltages and currents were acquired to process P_{IN} and P_{OUT}. The system accelerations were also measured.

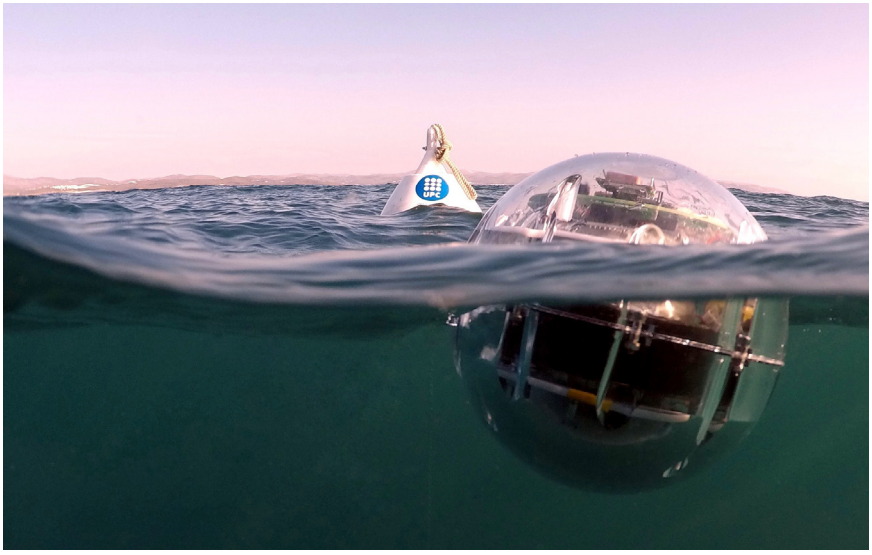

Figure 8. 20 cm, 3.6 kg spherical drifter with the embedded EH and monitoring systems during the deployment 4 km offshore from Vilanova i la Geltrú harbour. A white mooring buoy with the UPC logo indicates the fishing-protected area.

4. Results

4.1. First Test

In the first test, data were recorded for the duration of 5 min (300 s). Figure 9 (left) shows a 100 s time zoom of the drifter's linear accelerations with the horizontal accelerations A_X and A_Y plotted in red and green, respectively, and the vertical acceleration A_Z in blue. Figure 9 (right) shows the power spectral density obtained using the fast Fourier transform (with MATLAB) and using the 5-min data. A_X and A_Y had a peak-to-peak amplitude of 0.9 g, with a root-mean-square (RMS) value of 0.17 g each, and a predominant f_{EH} of 0.95 Hz, which is characteristic of the pendulum movement of the drifter caused by the displacement of the mass center from the geometric center. A_Z had a peak-to-peak amplitude of 0.5 g (with an offset of 1 g due to the gravity alignment), with an ac RMS value of 0.14 g, and a

predominant f_{EH} of 1.1 Hz, caused by the buoyancy vertical response of the drifter. These results are similar to those reported in [9] since the size and weight of the drifter were very similar, but some differences can be detected. First, the acceleration amplitudes were higher due to stronger swell conditions. Second, and most remarkably, the predominant f_{EH} (in A_X and A_Y) was 0.95 Hz, whereas 1.5 Hz was found in [9]. This difference was caused by a different weight distribution inside the drifter. In this test, the weights were placed around the WEC, resulting in an increase in the total vertical moment of inertia, whereas in [9], they were placed below the WEC. According to Equation (8) reported in [10], this reduces the horizontal f_{EH}. This shows that f_{EH} does not depend on the swell conditions, but on the drifter's shape and weight.

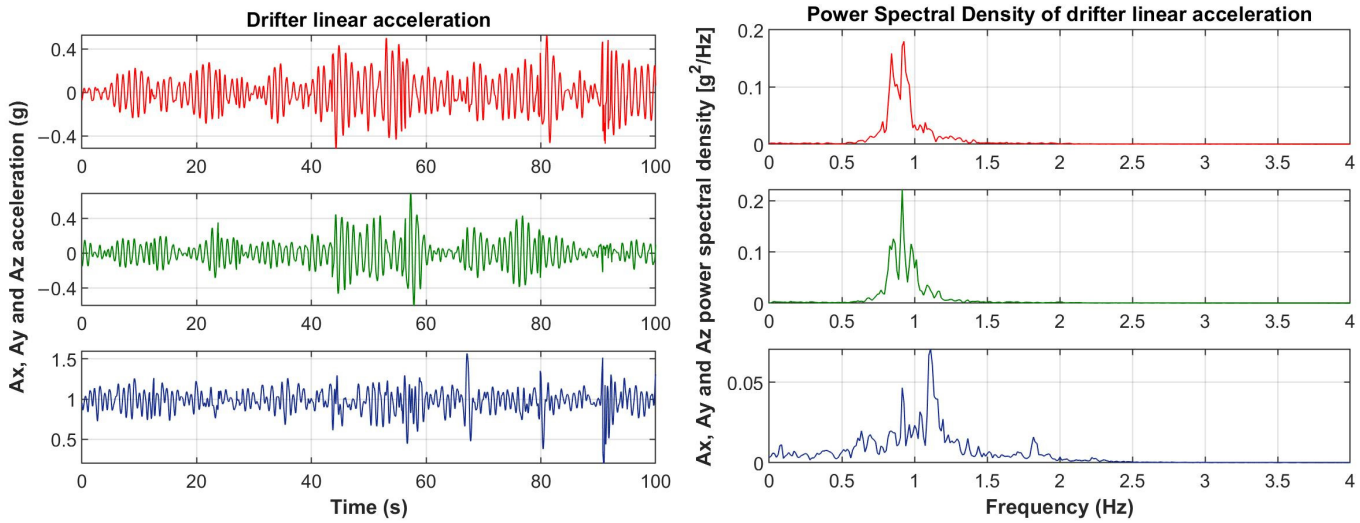

Figure 9. Experimental results of the first test at the sea. (**Left**) time series of the horizontal (A_X: red and A_Y: green) and vertical (A_Z: blue) accelerations of the drifter measured at the center of masses. (**Right**) power spectral densities of the linear accelerations.

Figure 10 shows V_{OC} for the full record of 5 min. The left plot (time domain) shows that V_{OC} had a pulsating behavior with spikes of up to 2 volts. Zero values were reached when the WEC's flywheel stopped its rotation. A predominant f_{EH} of 0.95 Hz was found in the frequency domain plot (right), in concordance with A_X and A_Y (Figure 9), because the pendulum arm of the WEC is mainly excited by the pendulum oscillation of the drifter. Consequently, a f_{MPPT} of 20.8 Hz (T_{MPPT} = 48 ms in Table 2) was chosen for config. C in the second test, so that $f_{MPPT} \approx 22 f_{EH}$, thus satisfying the condition for harvesting more than 99% of the maximum power [17]. A t_{SAMP} value of 57 µs was selected to have a small r_S (0.12 %), as shown in in Table 2, thus reducing the energy losses during t_{SAMP}.

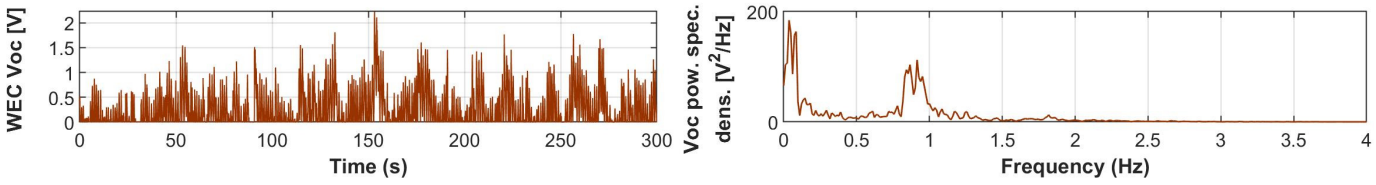

Figure 10. Experimental results of the first test at the sea. (**Left**) time series of the WEC's open circuit output voltage (V_{OC}) in V. (**Right**) power spectral density of V_{OC}.

4.2. Second Test

In the second test, data were recorded for the duration of 7.5 min (450 s). Figure 11 shows a 100 s time zoom of the horizontal (A_X: red and A_Y: green) and vertical (A_Z: blue) drifter's accelerations for both config. C and R. The RMS values of A_X and A_Y were between 0.17 g and 0.18 g in both cases, as were those measured in the first test. The RMS values

of A_Z were between 0.12 g and 0.14 g, again similar to those measured in the first test. Thus, swell conditions were similar between the first and second test, and between the consecutive tests for config. C and R within the second test. Figure 12 presents the full 7.5 min record of V_{GEN} (brown), P_{IN} (blue) and P_{OUT} (black) for config. C (left) and config. R (right). The tests for both configurations were consecutively performed.

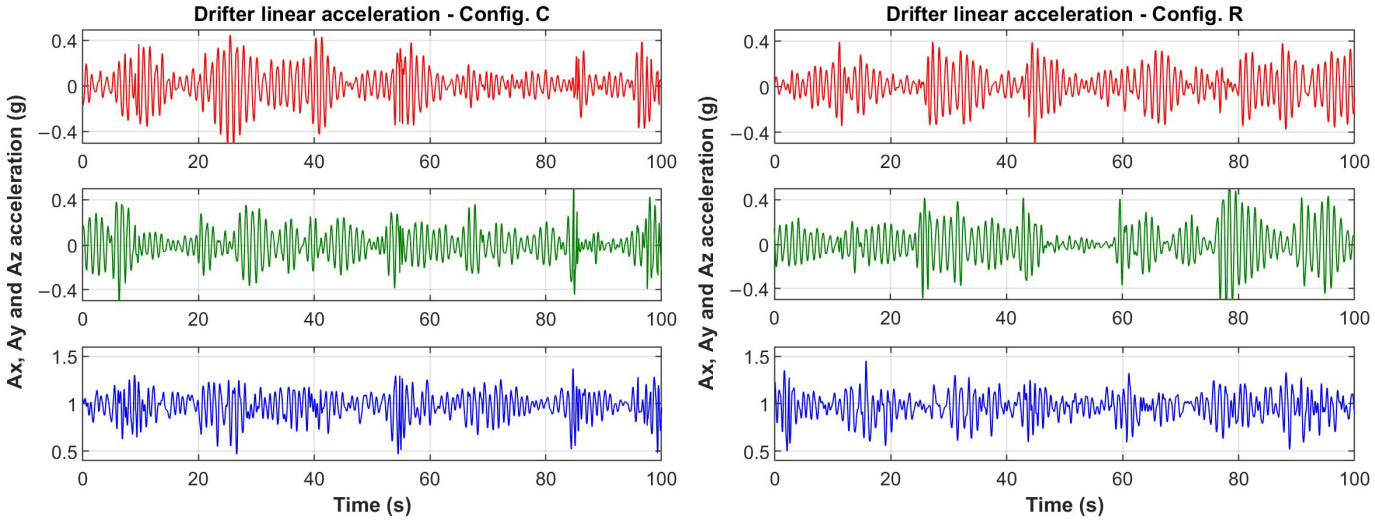

Figure 11. Experimental results for the second test at the sea. (**Left**) config. C. (**Right**) config. R. Both show the time series of the horizontal (A_X: red, and A_Y: green) and vertical (A_Z: blue) accelerations of the drifter.

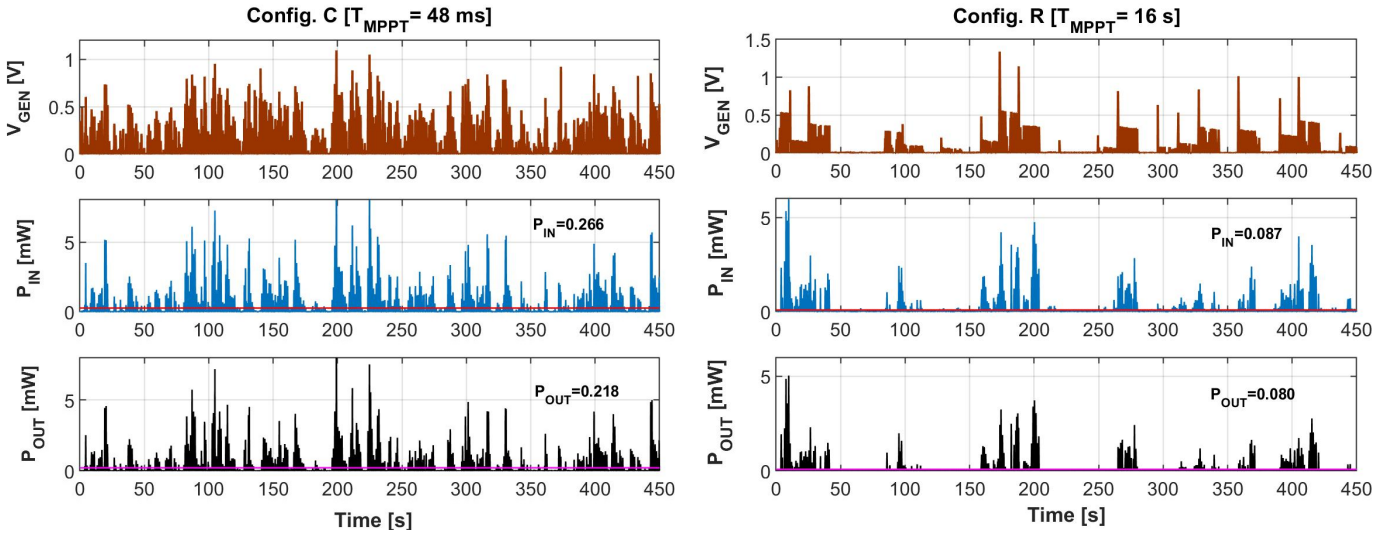

Figure 12. Experimental results for the second test at the sea. (**Left**) config. C with T_{MPPT} = 48 ms. (**Right**) config. R with T_{MPPT} = 16 s. Both show V_{GEN} (top, brown), P_{IN} (center, blue), $\overline{P_{IN}}$ (center, red), P_{OUT} (bottom, black) and $\overline{P_{OUT}}$ (bottom, pink) are represented.

For config. C, V_{GEN} reached peak voltages of up to 1 V, which corresponded to V_{OC} values of up to 2 V ($2V_{MPP}$), as shown in Figure 10 (left). As described in Section 2.2.2, in config. C, V_{OC} was not sampled. The frequency spectrum (not shown) was similar to that of Figure 10 (right). P_{IN} reached peak values of up to 10 mW, whereas the average (red line) was 266 µW. P_{OUT} peak values reached 9 mW, while the average (pink line) was 218 µW. Notice that not all of the generated useful power was delivered to the ESE because part was drained to feed the RO (17 µW at a f_{MPPT} of 20.8 Hz were measured in a preliminary test at the laboratory).

For config. R, V_{OC} and V_{MPP} showed peak values of approximately 1.4 V and 0.7 V, respectively, which were lower than those of config. C. One reason for this could be that no sample matched the maximum value of V_{OC} since the PMU was just sampling every 16 s. Furthermore, there were whole MPP cycles where V_{GEN} was fixed to zero and no energy was captured. This happened because the PMU sampled a V_{OC} of zero (V_{MPP} = 0 V) and the WEC was then short-circuited during the next 16 s. Overall, the average P_{IN} and P_{OUT} were reduced to 87 µW and 80 µW, respectively.

Table 3 summarizes the average power (P_{IN} and P_{OUT}) generated during the two tests. On the one hand, config. R only captured (P_{IN}) approximately 30% of the energy obtained with config. C. The reasons for this drop is the slow tracking of the MPP, which, according to [17], is a crucial factor. Table 3 also includes the efficiency (η) of both configurations. The efficiency of config. R was better than that of config. C (and close to that specified by the manufacturer of the ADP5092) because the latter included the consumption of the RO added to speed-up f_{MPPT} (≈17 µW at f_{MPPT} = 20.8 Hz). Even so, P_{OUT} was 2.7 times higher for config. C with respect to config. R.

Table 3. Comparison results of the power generation test on the marine environment.

Config	T_{MPPT}	P_{IN} (µW)	P_{OUT} (µW)	η (%)
C	48 ms	266	218	82
R	16 s	87	80	92

In [7], we estimated the possibility of feeding a low-power module, with sensing, processing and transmitting capabilities, from the energy produced by the WEC system. Specifically, a TD1205P capable of tracking the trajectory of the drifter in coastal areas and estimating the wave parameters using an accelerometer was selected. Since the energy used per transmitting cycle was 1.49 J, 12 transmissions per day would be feasible with the power generated during the sea test using config. C (218 µW) and just four using config. R (80 µW). Work is in progress to design a WEC with higher harvesting capabilities, and thus power a more power-demanding drifter such as the WAVY Ocean from MELOA [19].

Table 4 summarizes the main parameters of the results reported in [4–8], as well as those of the present work. For studies that used multiple technologies, only the electromagnetic-based results are reported. The table reports the WEC's technology and size (ϕ indicates diameter), the PMU type (custom or commercial), the MPPT method and sampling period, the test conditions and the output power density (in µW/cm^3). Power density was calculated by dividing the reported power by the calculated volume from the WEC's size. Suffixes a and p indicate average and peak values, respectively. The test conditions are indicated by the source type: simulation, laboratory or sea. The test conditions are quite different, so a fair comparison of the achieved power density is not possible. Even those carried out in a similar environment, e.g., at sea, present different excitations. Furthermore, in [5,6,8], power values are estimated or measured directly from the WEC output by estimating or using an optimum load resistor and without using the PMU. Therefore, the losses introduced by the PMU are not accounted for and it is assumed the WEC is operating at its MPP. However, in a practical system, this can only be achieved by using an MPPT with a fast-sampling rate, such as the one proposed in this study, and which is the focus of this work jointly with the test at the sea. In [7], the MPPT used was a slow MPPT based on config. R, as reported in this study, which produces, as shown in Table 3, suboptimal results.

Table 4. Results for electromagnetic-based, small-size WEC, harvesting energy from free floating buoys. The table includes the PMU used and the results achieved.

Ref.	Year	Technology	WEC Size (cm)	PMU	MPPT	Test	μW/cm^3
[4]	2022	Linear mov.	Cylinder 50 × 50ϕ	Not used	Not used	Sim	1.32a
[5]	2019	Swing body	Prism 10 × 10 × 6.3	Custom	Not used	Sea	206p
[6]	2022	Gimbal	Sphere 140ϕ	Custom	Not used	Lab	9.60p
[7]	2020	Double pendulum	Sphere 12ϕ	Commercial	FOCV, 16 s	Sea	0.198a/2.87p
[8]	2020	Double pendulum	Cylinder 16.7 × 10ϕ	Custom	Not used	Lab	0.94p
This work	2023	Double pendulum	Sphere 12ϕ	Custom	FOCV, 48 ms	Sea	0.241a/9.94p

5. Conclusions

In this article, the performance of FOCV-MPPT circuits has been evaluated using different sampling rates in a monitored sea area. To select the appropriate value for the sampling parameters, a small-scale, pendulum-type WEC was embedded in an oceanic drifter in order to estimate the f_{EH} of the WEC in OC under the effect of ocean waves. Results showed an f_{EH} of 0.95 Hz was produced by the pendulum motion of the drifter. In accordance with our previous studies, a suitable T_{MPPT} of 48 ms was selected. Then, a low-power control circuit was implemented using a RO to activate the fast sampling of V_{OC} on the MPPT. Finally, the performance of the fast-tracking FOCV-MPPT circuit was compared with a commercial PMU (T_{MPPT} of 16 s) on the same WEC and under similar sea condition. The results show that the fast-tracking FOCV-MPPT circuit reaches an average P_{IN} and P_{OUT} of 266 μW and 218 μW, respectively, while the slow-tracking FOCV-MPPT commercial circuit reaches 87 μW and 80 μW, respectively. Therefore, even accounting for the consumption of the control circuit (17 μW), the net harvested power is increased almost three times by speeding up the sampling rate of the MPPT circuit. With this amount of energy, it would be possible to feed a low-power node with sensing and transmitting capabilities of up to 12 messages per day in a coastal area. Previous studies did not use MPPT, so their reported maximum power cannot be achieved in practice.

Author Contributions: Conceptualization, M.C., A.S.H. and M.G.; methodology, M.C. and D.M.T.; software, M.C. and D.M.T.; validation, M.C., D.M.T. and J.d.R.; formal analysis, M.C., A.S.H. and M.G.; investigation, M.C., A.S.H. and M.G.; resources, M.C., D.M.T. and J.d.R.; data curation, M.C.; writing—original draft preparation, M.C.; writing—review and editing, M.C., A.S.H. and M.G.; visualization, M.C.; supervision, M.G.; project administration, J.d.R.; funding acquisition, J.d.R. All authors have read and agreed to the published version of the manuscript.

Funding: The first author was supported by the European Union—NextGenerationEU and the Ministerio de Universidades—Plan de Recuperación, Transformación y Resiliencia under a Margarita Salas post-doctoral research fellowship (ref. 2022UPC-MSC-94068). This work was partially supported by the project MELOA from the European Commission's Horizon 2020 research and Innovation program under Grant Agreement No. 776280. This study was developed using the framework of the Research Unit Tecnoterra (ICM-CSIC/UPC) and the following project activities: PLOME (PLEC2021-007525; Ministerio de Ciencia e Innovación) and BITER (PID2020-114732RB-C32; Ministerio de Ciencia e Innovación).

Institutional Review Board Statement: Not applicable.

Informed Consent Statement: Not applicable.

Data Availability Statement: Not applicable.

Acknowledgments: The authors would like to thank Marti Bartra for the pictures taken during the experimental test, some of which are shown in this article.

Conflicts of Interest: The authors declare no conflict of interest. The funders had no role in the design of this study; in the collection, analyses, or interpretation of data; in the writing of the manuscript; or in the decision to publish the results.

References

1. Poulain, P.M.; Gerin, R.; Mauri, E.; Pennel, R. Wind Effects on Drogued and Undrogued Drifters in the Eastern Mediterranean. *J. Atmos. Ocean. Technol.* **2009**, *26*, 1144–1156. [CrossRef]

2. Chen, J.; Bao, B.; Liu, J.; Wu, Y.; Wang, Q. Pendulum Energy Harvesters: A Review. *Energies* **2022**, *15*, 8674. [CrossRef]
3. Carandell, M.; Toma, D.M.; Pinto, J.P.; Gasulla, M.; del Rio, J. Impact on the Wave Parameters Estimation of a Kinetic Energy Harvester Embedded into a Drifter. In Proceedings of the IEEE OES/MTS OCEANS-Singapore and U.S. Gulf Coast, Biloxi, FL, USA, 5 October 2020; pp. 1–6. [CrossRef]
4. Harms, J.; Hollm, M.; Dostal, L.; Kern, T.A.; Seifried, R. Design and Optimisation of a Floating Wave Energy Converter for Drifting Sensor Platforms in Realistic Ocean Waves. *Appl. Energy* **2022**, *321*, 119303. [CrossRef]
5. Li, Y.; Guo, Q.; Huang, M.; Ma, X.; Chen, Z.; Liu, H.; Sun, L. Study of an Electromagnetic Ocean Wave Energy Harvester Driven by an Efficient Swing Body Toward the Self-Powered Ocean Buoy Application. *IEEE Access* **2019**, *7*, 129758–129769. [CrossRef]
6. Xue, F.; Chen, L.; Li, C.; Ren, J.; Yu, J.; Hou, X.; Geng, W.; Mu, J.; He, J.; Chou, X. A Static-Dynamic Energy Harvester for a Self-Powered Ocean Environment Monitoring Application. *Sci. China Technol. Sci.* **2022**, *65*, 893–902. [CrossRef]
7. Carandell, M.; Toma, D.M.; Carbonell, M.; del Río, J.; Gasulla, M. Design and Testing of a Kinetic Energy Harvester Embedded into an Oceanic Drifter. *IEEE Sens. J.* **2020**, *20*, 13930–13939. [CrossRef]
8. Chen, X.; Gao, L.; Chen, J.; Lu, S.; Zhou, H.; Wang, T.; Wang, A.; Zhang, Z.; Guo, S.; Mu, X.; et al. A Chaotic Pendulum Triboelectric-Electromagnetic Hybridized Nanogenerator for Wave Energy Scavenging and Self-Powered Wireless Sensing System. *Nano Energy* **2020**, *69*, 104440. [CrossRef]
9. Carandell, M.; Mihai Toma, D.; Gasulla, M.; del Río, J. Experimental Validation of a Kinetic Energy Harvester Device for Oceanic Drifter Applications. In Proceedings of the IEEE OES/MTS OCEANS-Marseille, Marseille, France, 17–20 June 2019; p. 17. [CrossRef]
10. Carandell, M. Contributions to the Design of Energy Harvesting Systems for Autonomous Sensors in Low Power Marine Applications. Ph.D. Thesis, Universitat Politècnica de Catalunya, Barcelona, Spain, 2022. Available online: https://upcommons.upc.edu/handle/2117/366910 (accessed on 6 March 2023).
11. Dondi, D.; Bertacchini, A.; Brunelli, D.; Larcher, L.; Benini, L. Modeling and Optimization of a Solar Energy Harvester System for Self-Powered Wireless Sensor Networks. *IEEE Trans. Ind. Electron.* **2008**, *55*, 2759–2766. [CrossRef]
12. Simjee, F.I.; Chou, P.H. Efficient Charging of Supercapacitors for Extended Lifetime of Wireless Sensor Nodes. *IEEE Trans. Power Electron.* **2008**, *23*, 1526–1536. [CrossRef]
13. Shao, H.; Li, X.; Tsui, C.Y.; Ki, W.H. A Novel Single-Inductor Dual-Input Dual-Output DC-DC Converter with PWM Control for Solar Energy Harvesting System. *IEEE Trans. Very Large Scale Integr. Syst.* **2014**, *22*, 1693–1704. [CrossRef]
14. Yu, C.G. A Vibrational Energy Harvesting Interface Circuit with Maximum Power Point Tracking Control. *Int. J. Appl. Eng. Res.* **2017**, *12*, 12102–12107.
15. Shrivastava, A.; Roberts, N.E.; Khan, O.U.; Wentzloff, D.D.; Calhoun, B.H. A 10 MV-Input Boost Converter with Inductor Peak Current Control and Zero Detection for Thermoelectric and Solar Energy Harvesting with 220 MV Cold-Start and −14.5 DBm, 915 MHz RF Kick-Start. *IEEE J. Solid-State Circuits* **2015**, *50*, 1820–1832. [CrossRef]
16. Balato, M.; Costanzo, L.; Lo Schiavo, A.; Vitelli, M. Optimization of Both Perturb & Observe and Open Circuit Voltage MPPT Techniques for Resonant Piezoelectric Vibration Harvesters Feeding Bridge Rectifiers. *Sens. Actuators A Phys.* **2018**, *278*, 85–97. [CrossRef]
17. Carandell, M.; Holmes, A.S.; Toma, D.M.; del Río, J.; Gasulla, M. Effect of the Sampling Parameters in FOCV-MPPT Circuits for Fast-Varying EH Sources. *IEEE Trans. Power Electron.* **2022**, *38*, 2695–2708. [CrossRef]
18. Thomas, R.E.; Rosa, A.J.; Toussaint, G.J. *The Analysis and Design of Linear Circuits*, 8th ed.; JOHN WILEY & SONS: Hoboken, NJ, USA, 2016; ISBN 0471386790.
19. MELOA Project. Available online: https://www.ec-meloa.eu/ (accessed on 31 March 2023).
20. Del-Rio, J.; Nogueras, M.; Toma, D.M.; Martínez, E.; Artero-Delgado, C.; Bghiel, I.; Martinez, M.; Cadena, J.; Garcia-Benadi, A.; Sarria, D.; et al. Obsea: A Decadal Balance for a Cabled Observatory Deployment. *IEEE Access* **2020**, *8*, 33163–33177. [CrossRef]